

See discussions, stats, and author profiles for this publication at: <https://www.researchgate.net/publication/266734714>

# Extending the Family of Tetrahedral Tectons: Phenyl Embraces in Supramolecular Polymers of Tetraphenylmethane-based Tetraphosphonic Acid Templatated by Organic Bases

ARTICLE *in* CRYSTAL GROWTH & DESIGN · OCTOBER 2014

Impact Factor: 4.89 · DOI: 10.1021/cg501348g

---

CITATIONS

4

---

READS

41

## 5 AUTHORS, INCLUDING:



[Michał Jacek Bialek](#)

University of Wrocław

10 PUBLICATIONS 37 CITATIONS

[SEE PROFILE](#)



[Jan Janczak](#)

Polish Academy of Sciences

264 PUBLICATIONS 2,788 CITATIONS

[SEE PROFILE](#)



[Jerzy Zoń](#)

Wrocław University of Technology

68 PUBLICATIONS 1,097 CITATIONS

[SEE PROFILE](#)



[Agnieszka Dobosz](#)

Wrocław Medical University

14 PUBLICATIONS 205 CITATIONS

[SEE PROFILE](#)

# Extending the Family of Tetrahedral Tectons: Phenyl Embraces in Supramolecular Polymers of Tetraphenylmethane-based Tetraphosphonic Acid Templatated by Organic Bases

Jan K. Zaręba,<sup>\*,†</sup> Michał J. Białek,<sup>‡</sup> Jan Janczak,<sup>§</sup> Jerzy Zoń,<sup>\*,||</sup> and Agnieszka Dobosz<sup>⊥</sup>

<sup>†</sup>Faculty of Chemistry, Wrocław University of Technology, 27 Wybrzeże Wyspiańskiego Street, 50-370 Wrocław, Poland

<sup>‡</sup>Department of Chemistry, University of Wrocław, 14 F. Joliot-Curie Street, 50-383 Wrocław, Poland

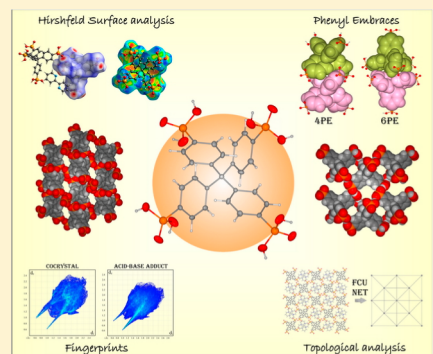
<sup>§</sup>Institute of Low Temperature and Structural Research, Polish Academy of Sciences, 2 Okólna Street, P.O. Box 1410, 50-950 Wrocław, Poland

<sup>||</sup>Department of Thermodynamics, Machine and Thermal Device Theory, Faculty of Mechanical and Power Engineering, Wrocław University of Technology, 27 Wybrzeże Wyspiańskiego Street, 50-370 Wrocław, Poland

<sup>⊥</sup>Department of Basic Medical Sciences, Wrocław Medical University, 211 Borowska Street, 50-556 Wrocław, Poland

## S Supporting Information

**ABSTRACT:** A missing member of the tetraphenylmethane-based family of supramolecular tectons, tetrakis(4-phosphonophenyl)methane, TPPM (**1**), has been obtained, characterized, and reacted with organic amines that possess modulated conformational flexibility. The obtained adducts serve as a diverse platform for the investigation of the amine templating effect on phenyl embraces, the resulting supramolecular network, and its topology. Hirshfeld surface (HS) analysis has been employed for the investigation of phenyl embraces, which led to the indication of characteristic HS features of 4PE and 6PE phenyl embraces. One can also observe a new subtype of phenyl embrace, namely, HBA-PE (hydrogen bond-assisted phenyl embrace), which constitutes the cooperation of two interactions: strong hydrogen bonding and a phenyl embrace. A topological insight into TPPM hydrogen-bonded networks is also provided. As a result, we found a connection of the amine template type with the periodicity of the underlying supramolecular network. Additionally, we report three previously unknown topologies. The obtainment of an unusual example of a phosphonic acid cocrystal with base (adduct **3**) allowed for the determination of specific 2D fingerprint plot patterns for acid–base structures, with and without proton transfer.



## INTRODUCTION

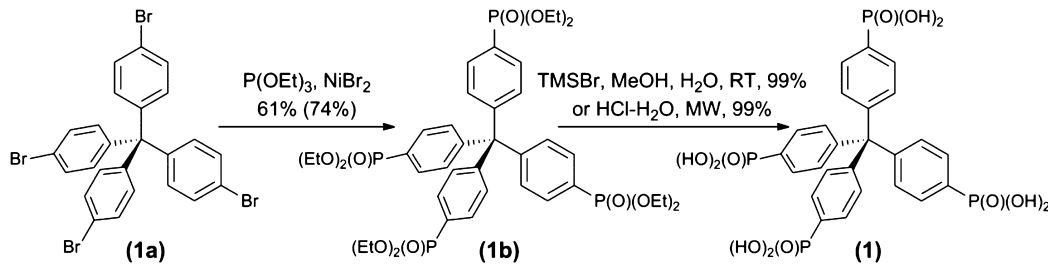
Supramolecular assemblies incorporating designed phosphonic acids are fascinating examples of molecular tectonics.<sup>1–8</sup> Considerable effort has been expended in recent years on attempts to understand the relationship between molecular structures of employed substrates and the crystal structure of the obtained solid.<sup>9–13</sup> However, accurate prediction of the crystal structures is still tricky, especially for substrates that can form diverse sets of intermolecular interactions.<sup>14–16</sup> Despite the fact that supramolecular chemistry of phosphonic acids is relatively unexplored for supramolecular assemblies of phosphonic acids with organic bases, to date some general rules have been established. One example is the strong tendency to form linear or layered structures resulting in dense and efficient packing in the solid state with proton transfer.<sup>17,18</sup> This leads to the creation of strong R<sub>2</sub>(8) binding motifs between the PO<sub>3</sub>H<sup>+</sup> groups in the same manner as in the case of the two COOH groups.<sup>13,18</sup> This is usually supported, where applicable, by a set of aromatic interactions.<sup>19</sup>

In terms of crystal engineering, there is a need for continuous design and synthesis of new challenging molecular models, while the most important issue involves testing how they behave in predefined new conditions. Although some organic skeletons are invariably fascinating for research purposes, the small group of tetrahedral motifs is of particular interest, with the tetraphenylmethane (TPM) skeleton taking the central position among them. There are three main routes for the alteration of a tetrahedral tecton structure: (I) modification of the tetrahedral core (e.g., Si,<sup>20,21</sup> B,<sup>22</sup> or bigger units like an adamantyl one<sup>23–26</sup> instead of the carbon atom), (II) an organic scaffold modification (substitution of benzene with pyridine<sup>27</sup> or elongation of an aromatic ring system<sup>28–31</sup>), and (III) functional group change (substitution of one for another,<sup>20,32,33</sup> symmetrization and application of a few different groups,<sup>34–36</sup> or change of substitution site<sup>37</sup>). To

Received: September 8, 2014

Revised: October 9, 2014

Published: October 10, 2014

**Scheme 1. Synthesis of Tetrakis(4-phosphonophenyl)methane (1, TPPM)**

date, tectons with a TPM core that have successfully found application in supramolecular and metal–organic framework chemistry are substituted with carboxylic,<sup>33,38–40</sup> sulfonic,<sup>25</sup> boronic,<sup>41</sup> and other nonacidic functional groups.<sup>20,32,42–44</sup> Surprisingly, a phosphonic analogue has been unknown in the literature so far. The only tetrahedral tetraphosphonic acid obtained and applied in crystal engineering has been tetrakis-1,3,5,7-(4'-phosphonophenyl)adamantane.<sup>1,2,26</sup> Thus, in order to extend the family of tetrahedral acidic TPMs and to increase the knowledge about rules governing assembly of phosphonic acids, we have synthesized the first tetraphosphonic acid based on tetraphenylmethane, namely, tetrakis(4-phosphonophenyl)methane (**1**, Scheme 1), and obtained a set of crystalline adducts with pyridine (**2**), 2,2'-bipyridine (**3**), 4-(*N,N*-dimethylamino)pyridine (DMAP) (**4**), 1,6-hexanediamine (**5**), and urotropine (hexamethylenetetramine, **6**) differing in the number of donors and conformational flexibility.

This research has three main aims: (1) to present a new tetrahedral phosphonic ligand, along with its optimized synthesis that allows for straightforward and efficient multigram synthesis, with no need for chromatography purification of the ester intermediate; (2) to conduct an investigation of the interactions responsible for acid–base adduct assemblies, by means of traditional analysis and Hirshfeld surface analysis, with particular focus on the influence of an organic base structure on the arrangement of acidic molecules; (3) to report multiple phenyl embraces present in these assemblies.

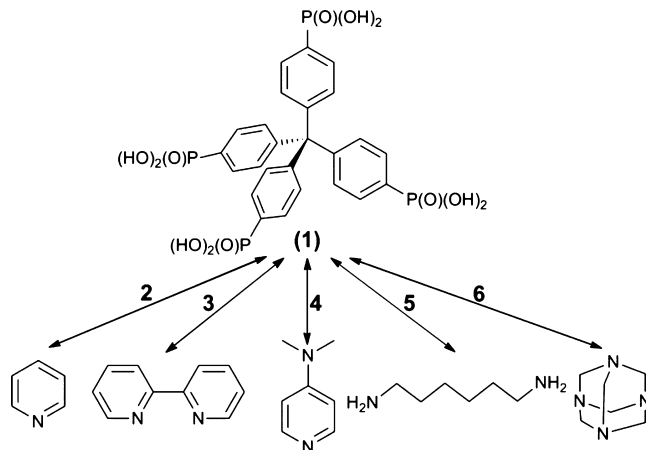
## EXPERIMENTAL SECTION

**Preparation of the Phosphonic Acid.** Tetrakis(4-phosphonophenyl)methane (**1**, TPPM) was obtained using a two-step method.<sup>45,46</sup> However, the procedure was optimized to furnish multigram quantities without the need for chromatographic separation. The newly obtained compounds were characterized by <sup>1</sup>H, <sup>13</sup>C{<sup>1</sup>H}, and <sup>31</sup>P{<sup>1</sup>H} NMR, IR, and HRMS (see Supporting Information for detailed description of experimental procedures and characterization, Figures S1–S8).

The tetrakis(4-bromophenyl)methane **1a** was subjected to nickel-catalyzed cross-coupling<sup>47,48</sup> with triethyl phosphite providing tetrakis[(4-diethoxyphosphoryl)phenyl]methane (**1b**). After a crystallization-based purification of a crude solid, ester **1b** was converted to the corresponding acid **1** via *trans*-silylation and subsequent methanolysis or, alternatively, microwave-assisted acidic hydrolysis. Scheme 1 summarizes the synthetic protocol of tetraphosphonic acid (**1**).

**Preparation of Adducts.** Adducts (**2–6**) were prepared via evaporation of solutions prepared by adding the acid to a base in the appropriate solvent system (see Supporting Information). An outline of supramolecular adducts prepared from N-containing organic bases and acid **1** is depicted in Scheme 2.

**X-ray Crystallography.** All the obtained single crystals were used for data collection on a four-circle KUMA KM4 diffractometer equipped with a two-dimensional CCD area detector. Graphite monochromatized Mo  $K\alpha$  radiation ( $\lambda = 0.71073 \text{ \AA}$ ) and the  $\omega$ -scan technique ( $\Delta\omega = 1^\circ$ ) were applied, while additional data collection

**Scheme 2. Building Units Used in This Article and the Symbols of the Structures**

and reduction, along with absorption correction, were performed using the CrysAlis software package.<sup>49</sup> The structures were solved by direct methods using SHELXS-97,<sup>50</sup> revealing the positions of all or almost all non-hydrogen atoms. The remaining atoms were located as a result of subsequent difference Fourier syntheses. The structures were refined using SHELXL-97<sup>50</sup> with anisotropic displacement parameters. For **2**, EXYZ together with EADP commands were used to resolve a pyridine molecule, which lies on the inversion center and thus is disordered over two positions. Hydrogen atoms connected to carbon atoms were constrained as a riding model. The positions of the H atoms of phosphonic groups, water molecules, and those connected to nitrogen atoms were located on a difference Fourier map and subsequently refined, where possible. In structure **5**, it was not possible to locate the hydrogen atoms in the water molecules, and in structures **4** and **6**, all located hydrogen atoms were constrained. Details of the data collection parameters, crystallographic data, and final agreement parameters are listed in Table 1. Selected geometrical parameters can be found in Table S1, Supporting Information. The geometry parameters of hydrogen bonds are listed in Table S2, Supporting Information. Visualization of the structures was conducted using the Diamond program,<sup>51</sup> while a topological simplification of HB networks was performed with the ToposPro package.<sup>52</sup> Some geometrical features of intermolecular interactions were determined with the help of Platon software.<sup>53</sup> Hirshfeld surface<sup>54,55</sup> and 2D fingerprint calculations<sup>56</sup> were performed using the Crystal Explorer package.<sup>57</sup> Crystal structures were imported from CIF files. By default, H–X bond lengths were set to neutron values. Hirshfeld surfaces were generated for acid molecules using very high resolution and mapped with shape index functions.

## RESULTS AND DISCUSSION

**Synthesis of Tetrakis(4-phosphonophenyl)methane (**1**, TPPM).** The straightforward synthesis, attractive geometry, and functions of tetrahedral tetraphosphonic acid **1** encourage undertaking detailed investigation of its supramolecular

Table 1. Crystal and Structure Refinement Data for All Adducts (2–6)

symbol of the structure	2	3	4	5	5b	6
empirical formula	C <sub>25</sub> H <sub>23</sub> O <sub>12</sub> P <sub>4</sub> , C <sub>5</sub> H <sub>6</sub> N <sub>2</sub> , 2(H <sub>2</sub> O)	C <sub>25</sub> H <sub>24</sub> O <sub>12</sub> P <sub>4</sub> , 2(C <sub>10</sub> H <sub>8</sub> N <sub>2</sub> )	C <sub>50</sub> H <sub>41</sub> O <sub>24</sub> P <sub>8</sub> , 6(C <sub>7</sub> H <sub>11</sub> N <sub>2</sub> ), 9(H <sub>2</sub> O), H <sub>3</sub> O	2(C <sub>25</sub> H <sub>21</sub> O <sub>12</sub> P <sub>4</sub> ), 2(C <sub>6</sub> H <sub>17</sub> N <sub>2</sub> ), 2(C <sub>6</sub> H <sub>18</sub> N <sub>2</sub> ), 9(H <sub>2</sub> O)	C <sub>25</sub> H <sub>17</sub> O <sub>12</sub> P <sub>4</sub> , 2(C <sub>6</sub> H <sub>18</sub> N <sub>2</sub> ), 2(H <sub>2</sub> O)	2(C <sub>25</sub> H <sub>20</sub> O <sub>12</sub> P <sub>4</sub> ), 4(C <sub>6</sub> H <sub>14</sub> N <sub>4</sub> ), 5(C <sub>2</sub> H <sub>6</sub> OS), 12(H <sub>2</sub> O)
formula weight	755.45	952.69	2193.82	1907.48	905.71	2418.07
cryst size [mm <sup>3</sup> ]	0.22 × 0.25 × 0.29	0.14 × 0.15 × 0.28	0.17 × 0.27 × 0.32	0.16 × 0.28 × 0.32	0.19 × 0.23 × 0.27	0.28 × 0.25 × 0.21
cryst syst	monoclinic	tetragonal	monoclinic	triclinic	triclinic	monoclinic
space group	C2/c	I4	C2/c	P1̄	P1̄	C2/c
a [Å]	24.640(4)	16.896(3)	28.564(4)	12.439(3)	13.597(4)	28.410(5)
b [Å]	6.887(2)	16.896(3)	14.585(3)	13.079(3)	13.866(4)	13.197(3)
c [Å]	21.583(4)	7.212(2)	24.855(4)	15.460(4)	15.312(5)	18.551(4)
α [deg]	90	90	90	78.48(3)	97.82(2)	90
β [deg]	118.10(4)	90	90.45(3)	69.40(3)	110.20(3)	123.74(5)
γ [deg]	90	90	90	89.50(4)	108.59(3)	90
V [Å <sup>3</sup> ]	3231.0(3)	2058.9(3)	10354.5(8)	2301.8(3)	2467.7(7)	5783.5(5)
Z	4	2	4	1	2	2
density (calcd) [Mg·m <sup>-3</sup> ]	1.553	1.537	1.407	1.376	1.220	1.389
F(000)	1568	988	4624	1014	928	2528
θ range [deg]	3.10–28.04	3.07–28.42	2.68–27.50	2.45–27.95	2.73–27.90	1.77–27.97
coeff, μ [mm <sup>-1</sup> ]	0.308	0.258	0.222	0.236	0.214	0.298
T [K]	295(2)	295(2)	295(2)	295(2)	295(2)	295(2)
λ [Å]	0.71073	0.71073	0.71073	0.71073	0.71073	0.71073
reflns coll., indep., obsd.	20475, 3888, 2690	8482, 2560, 1617	67381, 11864, 6734	30178, 10950, 5835	33544, 11697, 5909	24022, 6435, 4814
R <sub>int</sub>	0.0288	0.0724	0.0709	0.0583	0.0780	0.0225
data/params	3888/237	2560/153	11864/669	10950/582	11697/602	4814/6435
final R indices (I > 2σ(I))	R <sub>1</sub> = 0.0364, wR = 0.0918	R <sub>1</sub> = 0.0577, wR = 0.0886	R <sub>1</sub> = 0.0723, wR = 0.1337	R <sub>1</sub> = 0.0860, wR = 0.1016	R <sub>1</sub> = 0.0748, wR = 0.1372	R <sub>1</sub> = 0.0634, wR = 0.1550
R indices (all data)	R <sub>1</sub> = 0.0613, wR = 0.1075	R <sub>1</sub> = 0.1296, wR = 0.1164	R <sub>1</sub> = 0.1349, wR = 0.1650	R <sub>1</sub> = 0.2897, wR = 0.1469	R <sub>1</sub> = 0.1915, wR = 0.1647	R <sub>1</sub> = 0.0863, wR = 0.1729
GOF on F <sup>2</sup>	1.02	1.01	1.06	1.05	1.01	1.01
peak, hole [e·Å <sup>-3</sup> ]	0.32, -0.41	0.28, -0.27	0.39, -0.33	0.38, -0.38	0.82, -0.30	0.59, -0.50

behavior. Easy access to the acid samples is provided by the development of a multigram protocol for the synthesis of **1**. The synthesis begins with a well-described and easily obtainable precursor, tetrakis(4-bromophenyl)methane (**1a**),<sup>58,59</sup> and proceeds in two steps (Supporting Information). After the phosphorylation reaction of substrate **1a**, a purification process of the intermediate involves (I) precipitation of a crude octaethyl ester (**1b**) from the reaction mixture at a low temperature and (II) its dissolution in ethyl acetate and removal of all nickel contamination by oxidation of remaining Ni(0) with hydrogen peroxide and subsequent water extraction of Ni(II) salts.<sup>60</sup> Such a prepurified ester **1b** is then subjected to subsequent crystallizations providing a pure product with a yield of 61%. The additional chromatography of combined crystallization supernatants may provide an extra amount of ester, enhancing the total yield to 74%. This result is equivalent to almost 93% conversion calculated per one phosphonate group. Surprisingly, the preparation of tetraphosphonic acid **1** from **1b** via regular acidic hydrolysis (in conc. HCl) fails, providing a mixture of partially hydrolyzed derivatives of **1** as determined by <sup>31</sup>P{<sup>1</sup>H} NMR [four singlets from monohydrolyzed groups (around 16.3 ppm) and four singlets from fully hydrolyzed ones (around 11.8 ppm)]. The full conversion to tetraphosphonic acid is not achieved even after a prolonged hydrolysis time (up to 3 days). Nonetheless, microwave-assisted acidic hydrolysis under hydrothermal conditions is a

simple way to obtain complete hydrolysis. In standard conditions, partially hydrolyzed phosphonate groups generate a hydrogen-bond network strong enough to cause precipitation of the half-product and its elimination from the reaction environment.

Alternatively, a *trans*-silylation and methanolysis procedure provides pure **1** as an off-white solid with quantitative yield. The acid is only slightly soluble in water, alcohols, DMF, and DMA and sparingly soluble in acetonitrile; it is relatively well-soluble in boiling DMSO (15 mg/cm<sup>3</sup>). It seems that low solubility, even in polar solvents, is determined by a strongly hydrogen-bonded assembly, thus disfavoring acid molecule solvation. Extensive hydrogen bonding in the solid is confirmed by strong IR absorption in the range of 3800–2000 cm<sup>-1</sup>. Despite numerous efforts, **1** has been reluctant to give X-ray quality single crystals thus far.

**Structural Description.** The investigation of the supramolecular arrangement of acid **1** units was possible with the introduction of additional templating agents. In the course of establishing the influence of various N-containing organic bases on the final supramolecular arrangement of the tetrahedral acidic unit, we synthesized a series of crystalline adducts (2–6). At first, the reaction of **1** with bases containing a pyridine fragment allowed for the observation of extensive hydrogen bonding and aromatic interactions within a three-dimensional well-defined supramolecular network.

**Adduct of TPPM and Pyridine (2).** The asymmetric unit of **2** is composed of a half acid molecule, a half pyridine molecule disordered over two inversion-related positions, and one water molecule (Figure 1).

In the case of P1 groups, the P1–O2 bond is perpendicular to a phenyl plane, while for the P2 groups, the phosphoryl

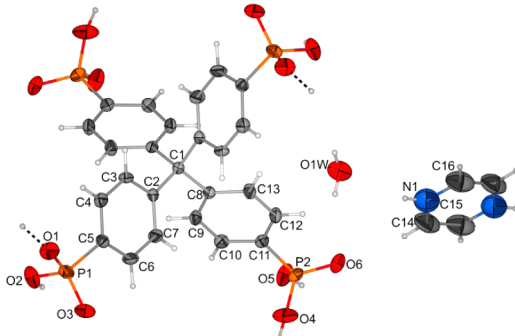


**Figure 1.** Asymmetric unit of adduct **2** (only atoms with labels). Displacement ellipsoids are drawn at a 50% probability level. Hydrogen atoms drawn arbitrarily small. A symmetric O1···H···O1 hydrogen bond marked with a dashed line. A disordered pyridine molecule lies on the inversion center.

oxygen atom (O6) lies in the plane of the phenyl ring. These two border conformations are stabilized by intramolecular interactions between the groups and the phenyl rings. Because, formally speaking, 1/2 of a proton per asymmetric unit is transferred to a pyridine molecule, there has to be one hydroxyl group with half proton occupation. The discussed proton lies on the inversion center, generating a symmetric hydrogen bond with O1···O1' distance of 2.469(3) Å. The symmetric HB generated in a molecule with 2-fold symmetry together with its equivalent provide a strong polymeric chain along the *c* axis.

Concerning intermolecular hydrogen bonding, the foregoing pattern provides a set of seven hydrogen bonds (Table S2, Supporting Information). Besides the supramolecular chain, O–H···O hydrogen bonds create two ring motifs that can be described, according to graph set theory notation,<sup>61</sup> as R<sup>3</sup>(12) and R<sup>4</sup>(14). The water molecule acts as a double donor and a single acceptor of HB and performs a supportive role in both rings. Such motifs, together with 2-fold screw axis-related fragments, provide a hydrogen-bonded tape along the *b* axis (marked gray-green; Figure 2). This tape is connected with others by symmetric hydrogen bonding and tetrahedral linkers giving a three-dimensional supramolecular network (Figure 3).

Protonated base molecules are placed inside small channels generated in the acidic framework along the *b* axis. The pyridine rings are connected to O3 through an N–H···O bond acting as pendants in the structure, as expected. There are additional stabilizing C–H···π interactions with phenyl rings above and below the pyridine ring with an 84.80(9)° angle between the pyridine and phenyl ring planes.

**Adduct of TPPM and 2,2'-Bipyridine (3).** Extending our studies to two pyridine rings connected by a single bond that allows only limited conformational changes, we obtained an intriguing example of a phosphonic acid cocrystal. Despite the final lack of a proton transfer, 2,2'-bipyridine enables dissolution of the acid in water and directs, at least partially, the assembly of a cocrystal structure. The asymmetric unit is composed of a quarter of the acid and a half of the 2,2'-bipyridine (Figure S9, Supporting Information), which is

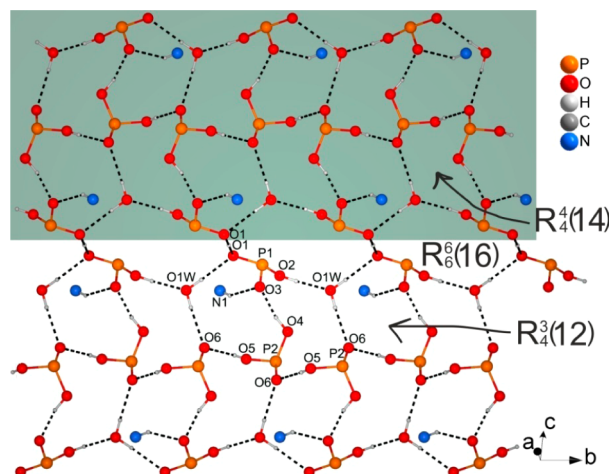


**Figure 2.** Presentation of adduct **2** HB network. One unique HB tape is marked with the gray-green plane. Tapes created from multiplied R<sup>3</sup>(12) and R<sup>4</sup>(14) motifs are connected by an additional R<sup>6</sup>(16) motif involving symmetric hydrogen bonding. Dashed lines symbolize hydrogen bonds.

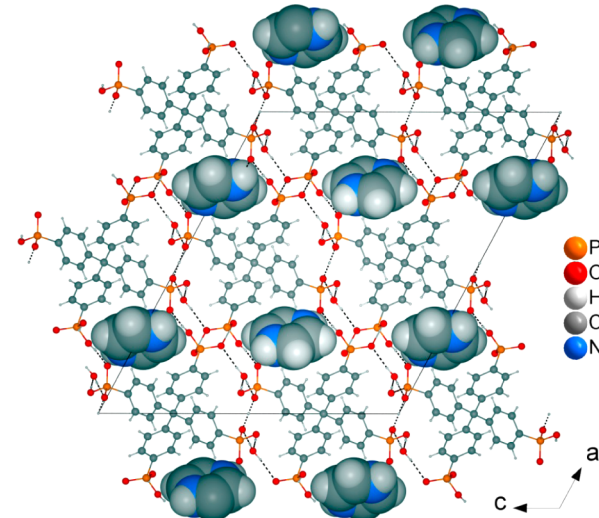


**Figure 3.** Three-dimensional HB network in adduct **2** crystal presented along the [010] direction. Base molecules residing in [010] channels are shown using a space-filling model with arbitrarily chosen atomic radii. Dashed lines symbolize hydrogen bonds.

enabled by the tetragonal noncentrosymmetric space group  $\bar{I}4$ . Despite the relatively high acidity of TPPM during the first deprotonation step ( $pK_{a1} < 2.36$ , see Supporting Information for potentiometric studies of TPPM), a proton is not transferred onto the nitrogen atoms.<sup>62</sup> This is probably because 2,2'-bipyridine is a weak base with  $pK_a$  equal to 4.46<sup>63</sup> vs 5.22<sup>64</sup> for pyridine. Adducts of organic acids, for example, phosphonylated calixarene, with free, unprotonated 2,2'-bipyridine are known in the literature.<sup>65</sup>

Twisted conformation of base molecules changed their role in the adduct. 2,2'-Bipyridine is a connector between 2-fold axis-related hydroxyl groups (O2) from neighboring unit cells. This interaction, symmetrically developed in the *a* and *b* directions, binds tetrahedral TPPM nodes, and together they create a very elegant supramolecular system, in which base molecules are situated inside 4-fold symmetry-related channels running along the *c* axis (Figure 4). Direct hydrogen bonding

between the 2-fold screw axis-related phosphonic groups builds a crystal in the [001] direction generating a C(4) motif ( $P\bar{1}$ –O3–H<sub>2</sub>O…O1).

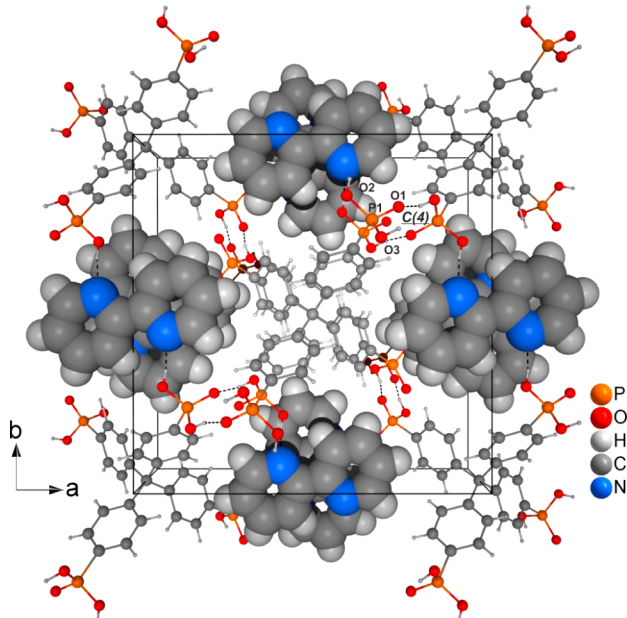


**Figure 4.** Supramolecular framework in adduct 3 shown along the [001] direction. Base molecules shown using a space-filling model with arbitrarily chosen atomic radii reside inside [001] channels laid perpendicularly. Dashed lines symbolize hydrogen bonds. The C(4) motif is presented in a perspective with participating atoms marked.

**Adduct of TPPM and 4-(*N,N*-Dimethylamino)pyridine (4).** A structure with a pyridine derivative substituted in the *para* position with a bulky aliphatic fragment, that is, 4-(*N,N*-dimethylamino)pyridine (DMAP), produced a very different result. The asymmetric unit of the obtained adduct consists of one TPPM molecule, three DMAP molecules, and six water molecules (Figure S10, Supporting Information). Therefore, the unit cell is much more “chaotic” and also larger than in previous cases ( $>10000 \text{ \AA}^3$  vs  $>3000 \text{ \AA}^3$  for 2).

The TPPM molecule transferred three protons to pyridinic nitrogen atoms, so the fourth phosphonic group should remain doubly protonated. Nevertheless, here we have another example of a symmetric hydrogen bond between inversion-related groups (the O42…O42' distance is 2.446(4) Å), producing strongly bonded dimeric secondary units. Such units are connected into a network via hydrogen bonds donated and accepted by the phosphonic groups and water molecules. Among others, strong  $R_2^2(8)$  motifs expected for  $\text{PO}_3\text{H}^-$  groups are present (Figure 5). The DMAP molecules perform the role of pendants connected to two phosphonic oxygen atoms (O11, O21) or one water molecule (OSW). Together, a very complex three-dimensional network is generated (Figure S11, Supporting Information).

**Adduct of TPPM and 1,6-Hexanediamine (5).** In the course of establishing the relationship between the structure of the templating base and the complexity of the obtained network, we sought a base with high lability and the potential for dispersive interactions (more than in DMAP). We conclude this is the reason for obtaining less well-defined structures. In order to investigate this relationship, we have obtained and

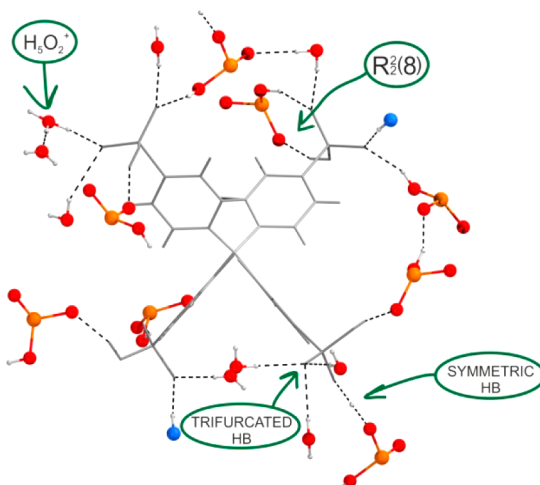


**Figure 5.** An outline of the most important features of the supramolecular environment around the TPPM molecule for adduct 4. A numerous set of hydrogen bonds (marked by dashed lines) creates a complicated supramolecular network.

examined a monocrystalline product of the reaction involving TPPM and 1,6-hexanediamine.

The structure of the obtained adduct shows many similarities to structure 4 (with DMAP), including a common triclinic  $P\bar{1}$  space group. However, the most important shared feature is the composition of the asymmetric unit. It is composed of one acid molecule with three base parts (one full base molecule and two halves), and five water molecules (Figure S12, Supporting Information). All three independent base fragments are protonated; thus TPPM is triply deprotonated in this adduct. Again, one can notice a high diversity of independent species providing a less well-defined network of interactions. Two of the three 1,6-hexanediamine molecules together with the water molecules reside inside the channels generated along the [010] direction. The third base molecule separates the acid molecules and lies approximately perpendicularly to the *b* axis (Figure 6).

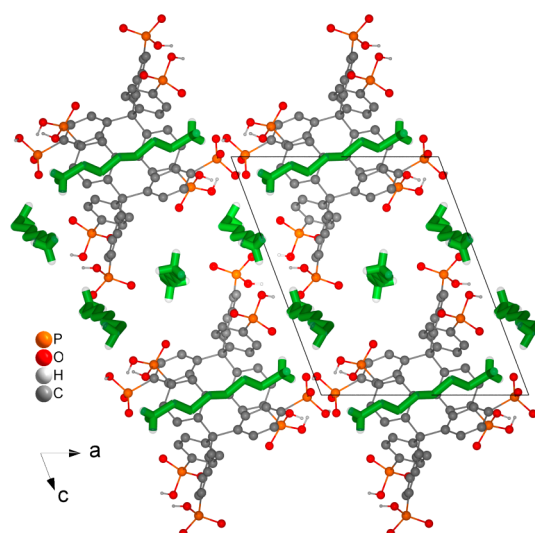


**Figure 6.** Molecular packing in adduct 5 crystal shown along the [010] direction. One can see base molecules (marked green) shown in the wire mode lying inside the [010] channels and other ones parallel to the (010) plane. Hydrogen atoms (except ones involved in HBs) and water molecules removed to increase the clarity of the figure.

It was not possible to locate water protons. Nevertheless, the overall donor–acceptor pattern with O···O distanced in the range between 2.488(6) and 3.110(10) Å (2.745(5)–3.171(6) Å for N···O ones) furnishes the three-dimensional architecture of a hydrogen bond network. The shortest O···O distance suggests the presence of a strong, perhaps symmetric, hydrogen bond. Such systems, in which bulky, rigid units produce a framework filled with differently interacting species (with a high dispersion contributor), are vulnerable to conformational changes that lead to solvato- or polymorphism. This is the case for **5**. The data collected for one of the polymorphic forms (**5b**) confirm this statement (see Table 1 and Supporting Information), yet it showed a severe disorder of the phosphonic groups and solvent molecules. In contrast to such labile structures, ones with well-defined networks, such as **2** or **3**, show higher reproducibility and uniformity.

**Adduct of TPPM and Urotropine (6).** The use of irregular, monobasic templates (DMAP) or ones with significant conformational freedom (1,6-hexanediamine), all with increased propensity for dispersion interactions, produced the jumbled structures **4** and **5**. A combination of dispersive “chaos” with a well-defined fixed unit led to the obtainment of a structure of TPPM with urotropine. This resulted in a 1:2 adduct. The asymmetric unit consists of a half acid molecule with each group monodeprotonated and a base molecule doubly protonated. Additionally, there are disordered DMSO and water molecules present (Figure S13, Supporting Information). A supramolecular network is well-defined by acid molecules. The first unique phosphonic group (P2) binds with the inversion-related group creating a R<sub>2</sub><sup>2</sup>(8) motif. The third oxygen atom (uninvolved in the motif, O21) binds to the second unique group (P1). This group is also connected to urotropine with a single N1–H···O12 bond. Such a pattern of connectivity provides a 2D TPPM network parallel to the (100) plane (Figure 7).

The second proton from the base molecule is connected with a disordered water molecule (N3–H···O3W/O4W), producing further connectivity in the [100] direction. Nonetheless, it cannot be fully established due to the severe disorder of this

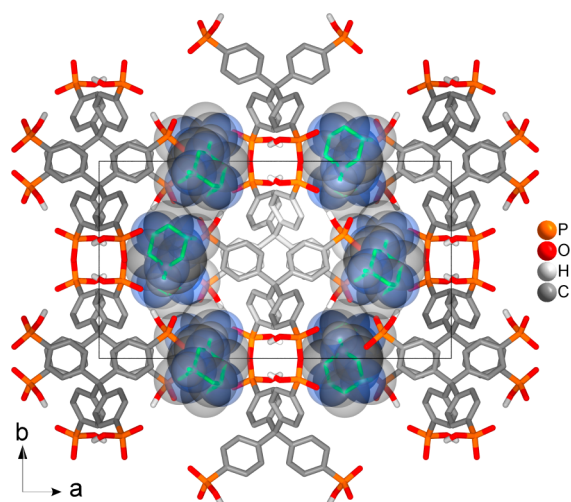


**Figure 7.** A supramolecular framework of adduct **6** shown along the [001] direction. One can see base molecules (the semitransparent space-filling molecules) residing between (100) sheets made by the TPPM molecules (presented with the wire mode). Solvent molecules are removed to increase the clarity of the figure.

water molecule. DMSO molecules reside in small void spaces within the framework. These solvent molecules can affect the overall structure preventing connection in the third dimension,<sup>13</sup> due to extensive dispersion interactions from methyl groups.

**Relations between Phenyl Scaffolds: Phenyl Embraces in Adducts of Tetrahedral Tetraphosphonic Acid and the Templating Effect.<sup>66</sup>** The discussed phosphonic acid has a tetraphenylmethane core, which determines its susceptibility for forming phenyl embraces, and indeed, this is the case for compounds **2**–**5**. Apart from careful viewing of the structures in order to identify the presence and kind of phenyl embraces, we calculated geometrical parameters such as the shortest distance between central atoms of tetraphenylmethane units  $d(C_{\text{ipso}}\cdots C_{\text{core}})$  and the mean colinearity angle  $\alpha(C_{\text{ipso}}\cdots C_{\text{core}}\cdots C_{\text{core}})$ .<sup>67,68</sup> The results and determined phenyl embraces have been collected in Table 2.

**Table 2. Geometrical Parameters Used For Determination of Phenyl Embraces**

structure	$d(C_{\text{ipso}}\cdots C_{\text{core}})$	$\alpha(C_{\text{ipso}}\cdots C_{\text{core}}\cdots C_{\text{core}})$	phenyl embrace
<b>2</b>	6.839(3)	126.9(2)	4PE
<b>3</b>	7.212(5)	127.0(1)	4PE
<b>4</b>	6.338(5)	176.7(2)	6PE
<b>5</b>	6.118(5)	176.5(2)	6PE
<b>6</b>	9.859(5)	<i>a</i>	none

*a*Not applicable.

Comparatively longer distances between central atoms (in the range of 6.8–7.4 Å),<sup>66d</sup> as well as a colinearity angle lower than 130° for adducts **2** and **3**, clearly indicate a 4PE interaction between tetrahedral units; each acidic unit participates in two 4-fold phenyl embraces with neighboring molecules, which provides infinite linear columns propagating along [010] and [001] directions, respectively (Figure 8). The distances between central atoms are equal to the length of respective periods.

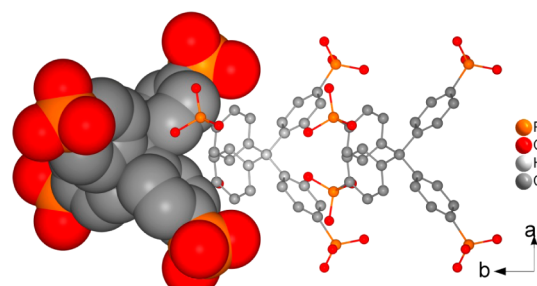


**Figure 8.** Columnar assembly of TPPM molecules of adduct **2** presenting the 4PE synthon shown along the [001] direction. One TPPM molecule shown using a space-filling model with arbitrarily chosen atomic radii. The other two are ball-and-stick representations.

It is interesting how these columns are packed within the crystal. Translational columns in **2** have a pseudohexagonal environment (Figure S14, Supporting Information); each 4PE-held row is connected via strong hydrogen bonds with six other adjoining columns. The shortest distances between these rows amount to 10.792(6), 11.958(6), and 12.320(6) Å. Such a way of packing the rows gives rise to channels that are occupied by pyridine molecules.

A different row environment is found when the 2,2'-bipyridine adduct (**3**) is considered, which results from the tetragonal crystallographic system. Each column has a hydrogen-bond contact with four surrounding columns, with a distance between them equal to 11.947(5) Å. Due to a noncentrosymmetric space group, these rows are arranged in a parallel fashion, while in **2** the rows are aligned in an antiparallel manner (Figure S15, Supporting Information). The imposed 4-fold symmetry results in less efficient packing of the rows but renders a larger void space that allows for a bigger 2,2'-bipyridine molecule to reside in it.

It is worth noting that pyridine and 2,2'-bipyridine efficiently fill the channels in both adducts, leaving almost no space for crystallization solvents. It seems that simple aromatic bases without functional groups, which introduce steric hindrance, fit well inside channels, privileging the formation of 6PE-held linear columns.

The 4PE structural motif in the adduct is not induced when bases have a propensity for increased dispersive interactions with the environment. In such cases, 6PE or large-ring motifs are formed instead. Nearly colinear geometry (within a 160–180° range), in conjunction with shorter  $C_{\text{core}}-C_{\text{core}}$  separations (5.8–6.8 Å), is diagnostic of 6PE interaction in structures with 4-(*N,N*-dimethylamino)pyridine (**4**) and 1,6-hexanediamine (**5**). Acid molecules from dimeric propellor-like units with pseudo-3-fold symmetry do not fill the void spaces efficiently. They are not, however, isolated from each other: in **4**, dimeric units are connected via  $R_2^2(8)$  motifs in the [010] direction and are held by symmetric hydrogen bonds in the [001] direction. The empty space between the dimeric units is occupied by 4-(*N,N*-dimethylamino)pyridine and water molecules (Figure 9).

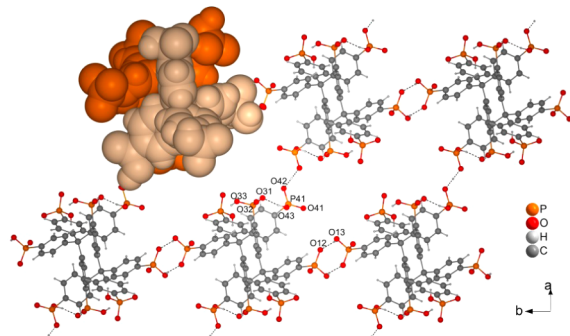


**Figure 9.** Dimeric assembly of TPPM molecules of adduct **4** presenting 6PE interaction shown along the [001] direction. Two molecules participating in a unique dimer are shown as space-filling models (orange and beige). The other ones are ball-and-stick representations. Dashed lines symbolize hydrogen bonds with participating atoms labeled.

In **5**, 6PE-held units seem to be packed comparatively more closely than those in **4**, which can be considered to be a consequence of the rod-like shape of the 1,6-hexanediamine templates (Figure S16, Supporting Information). In this compound, the 6PE dimers lie closer to each other: the 6PE units are connected in the [010] direction through two centrosymmetrically related O13–H···O21 hydrogen bonds. Dimeric units are extended into a hydrogen-bonded network primarily through the  $R_2^2(8)$  motif in the [100] direction as well as with the auxiliary O43–H···O32 hydrogen bond created with the same phosphonic group (P31).

A common feature of these structures is the lack of the base molecules' shape complementarity to the supramolecular network defined by 6PE-held dimers. When an empty space cannot be filled efficiently with amine compounds, then assembly of the 6PE interaction is preferred. The most probable explanation for this fact is an aliphatic-fragment-rooted bulky shape with an irregular surface of the used bases. This results in reduced capability to form more directional interactions with an acid's aromatic scaffold. As a side effect, a significant amount of crystallization solvent molecules are present.

The structure incorporating urotropine (**6**) is the only one in which phenyl embraces are precluded. Here, each tetraphosphonic acid TPPM binds directly via two phosphonic groups with two neighboring molecules, resulting in a supramolecular chain propagated along the [001] direction composed of large rings. DMSO molecules lie between the arms of TPPM molecules, strongly altering the final set of interactions. Thus, adjoining molecules interact using only strong hydrogen bonds and are significantly separated ( $C_{\text{core}}-C_{\text{core}}$  distance of 9.859(5) Å), far beyond the upper limit expected for phenyl embraces (7.4 Å). These chains are further bridged by the  $R_2^2(8)$  motif in the [010] direction, generating a 2D sheet, and thus the two formed differently sized supramolecular channels are occupied by DMSO, water, and urotropine molecules (Figure 10). The

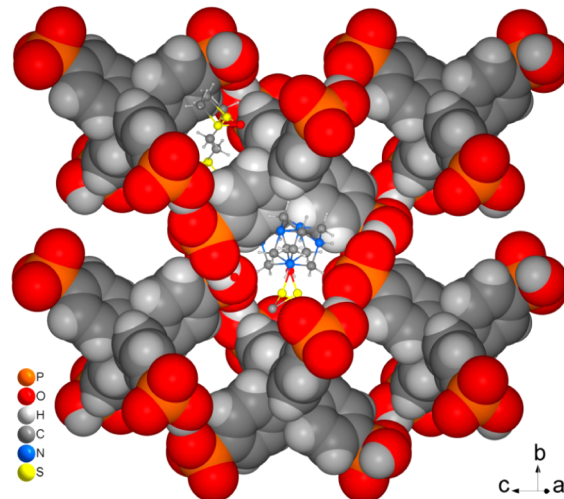


**Figure 10.** Two-dimensional hydrogen-bonded network of TPPM molecules in adduct **6**. TPPM molecules shown using a space-filling model with arbitrarily chosen atomic radii. There are two channels of different size, the bigger one occupied by base and disordered solvent molecules and the smaller one filled only with disordered solvent molecules. Urotropine and solvents occupying supermolecular channels are shown using ball-and-stick representations.

overall structure **6** constitutes a combination of dispersion interactions provided by DMSO and nearly spherically shaped urotropine molecules with a well-defined anionic framework of the TPPM molecules.

**Hirshfeld Surface Properties of 4PE and 6PE Phenyl Embraces.** An additional valuable and informative comparison of phenyl embrace motifs can be provided by means of Hirshfeld surface (HS) analysis.<sup>69</sup> Because phenyl embraces herein shown are constructed from edge-to-face C–H···π interactions, for visualization of representative examples of these two types of motifs, we applied a C···H decomposed

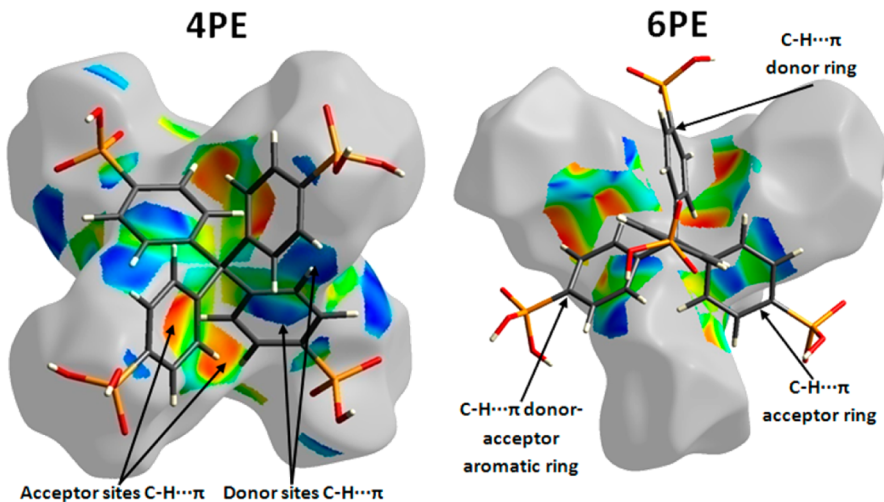


**Figure 11.** C–H decomposed shape index-mapped Hirshfeld surfaces for 4PE (left) and 6PE (right) phenyl embraces. Acceptor sites of this interaction are colored red, while donor sites are shown in blue.

shape index mapped HS, since they are best suited for this purpose. The 4PE interaction is represented as a set of four groups of elongated doubled spots (blue or red) that resulted from edge-to-face interactions of only two aromatic rings. Because each molecule is engaged in two 4PEs, the whole molecule forms eight donor and acceptor C–H–π interactions with its surroundings (Figure 11).

While in the 4PE motif the spot pattern is of 2-fold symmetry, in 6PE no symmetry of a shape index array can be found, despite the apparent pseudo-3-fold symmetry of the dimeric unit (Figure 11). Here, one phenyl ring serves simultaneously as a donor and acceptor of edge-to-face interactions while the remaining two phenyl rings act almost exclusively as C–H–π donors or C–H–π acceptors. Overall, the 6PE dimeric motif is composed of four donor and four acceptor C–H–π interactions (four red and four blue spots on the acid Hirshfeld surface).

Both types of phenyl embraces also differ with respect to the geometry of the edge-to-face C–H–π interactions from which they are built. In 6PE, a smaller angle between interacting phenyl rings results in more elongated red and blue spots on the shape index mapped HS, whereas for 4PE these spots are more roundly shaped, indicating an interaction angle closer to orthogonality.

**Hydrogen Bond-Assisted Phenyl Embrace (HBA-PE).** The 6-fold phenyl embrace (6PE) encountered in the adduct with DMAP (4) is not the only interaction effectively holding tetraphenylmethane units together. Closer examination of 6PE dimer molecules shows that apart from the 6PE interaction there are two inversion-related strong hydrogen bonds (O43–H–O31) between phosphonic groups within this dimer (Figure 12). Such a cooperative combination of attractive interactions should be particularly stabilizing.

Intriguingly, a CSD search<sup>70</sup> revealed no examples of cooperation between strong hydrogen bonding and phenyl embraces of any kind. This led to the conclusion that the HBA-PE is limited to molecules in which functional groups have the ability to be hydrogen-bonded simultaneously. Phosphonic and sulfonic acids seem to be tailored for HBA-PE motif generation due to their tetrahedral shape and multiple hydrogen-bonding character. The boronic functional group is planar like the carboxylic one, although the former has two protonated oxygen

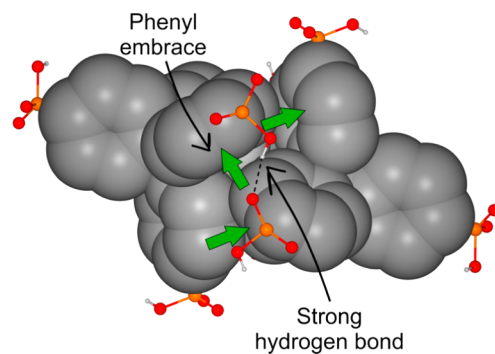


**Figure 12.** Projection showing the idea behind HBA-PE (hydrogen bond-assisted phenyl embrace). Green arrows denote edge-to face C–H–π interactions constituting a phenyl embrace, while the dashed line symbolizes the hydrogen bond.

atoms, which extends possible binding modes and suggests the ability to form the HBA-PE motif. Considering the geometry of the phenyl embrace itself, we suppose that the HBA-PE combined interaction can be preferentially found in systems incorporating 6PE, because in this motif the functional groups are situated roughly in the same plane due to 3-fold interdigitation. Therefore, the distance between functional groups is shorter than that for 4PE.

**Topological Analysis of Hydrogen-Bonded Networks.** We performed an analysis of obtained adduct structures using the TOPOS application, in order to gain some insight into the topology of hydrogen-bonded frameworks constructed from a TPPM building block in dependence of an accompanying base. To analyze the connectivity pattern between acid molecules, we calculated topological parameters taking only TPPM building blocks as nodes (TPPM net). For completeness of study, we established topological parameters for hydrogen-bonded nets containing not only TPPM molecules but also additional connecting nodes: water, 2,2'-bipyridine, and 1,6-hexamethylene diamine for 2, 3, and 5, respectively (Table 3). We neglected water molecules as nodes in adducts 4, 5, and 6 due to their large amounts in the crystal lattice. Taking them into account would have led to the identification of unnecessarily complex multinode topologies.

Table 3. Summary of Determined Topologies of Hydrogen-Bonded Nets in Adducts 2–6

structure	phenyl embrace	topology of TPPM net	additional nodes	topology of HB network involving TPPM and additional nodes
2	4PE	pcu	water	2-n, 3,12-c, PS: $(4^{36}.6^{27}.8^3)(4^3)_2$
3	4PE	bcu	2,2'-bipyridine	fcu
4	6PE	1-n, 7-c, PS: $(3^6.4^6.5^3.6^6)$ (underlying net hxl)		
5	6PE	sql	1,6-hexanediamine	3-n, 3,6,11-c, PS: $(3^2.4^7.5^6)(3^5.4^{20}.5^{14}.6^{15}.7)_2(4^3)_2$
6	none	sql		

In adduct **2**, TPPM molecules are six-connected between themselves, according to pcu (primitive cubic) topology. Consideration of the water molecule as an additional node gives rise to an unknown topology featured by net point symbol  $(4^{36}.6^{27}.8^3)(4^3)_2$ , wherein  $(4^{36}.6^{27}.8^3)$  and  $(4^3)$  notations correspond to TPPM and water molecule nodes, respectively. In adduct **3**, the TPPM molecules are eight-connected nodes, according to bcu (body-centered cubic) topology. Incorporation of 2,2'-bipyridine introduces four links per one TPPM node providing a well-known 12-connected fcu (face-centered cubic) topology.

A recent paper concerning hydrogen-bonded two-periodic nets<sup>71</sup> showed that the most often encountered nodes are three- and four-connected. The same is true in the case of adducts **5** and **6**, in which TPPM molecules are four-connected, resulting in sql (square lattice) topology. Interestingly, in the case of adduct **4**, an unprecedented uninodal, 7-connected, 3-periodic net is present. This net can be described by point symbol  $(3^6.4^6.5^3.6^6)$ . However, further simplification of the network by neglecting a symmetric hydrogen bond connecting the layers of the TPPM molecules gives rise to the common hxl (hexagonal close-packed layer) topology. Thus, the underlying topology of the TPPM network in **4** is essentially two-periodic. Topological determination of structure **5**, involving 1,6-hexanediamine molecules as nodes, leads to an unknown, rather complicated 3-nodal net defined with point symbol  $(3^2.4^7.5^6)(3^5.4^{20}.5^{14}.6^{15}.7)_2(4^3)_2$ . Here, the  $(3^5.4^{20}.5^{14}.6^{15}.7)$  notation matches the TPPM node, while  $(3^2.4^7.5^6)$  and  $(4^3)$  indices match two different kinds of 1,6-hexanediamine nodes.

## CONCLUSIONS

Our present study introduces an efficient and simple synthetic methodology for a new tetrahedral tetraphosphonic building block.

It can be observed that bases with bulky, flexible fragments are prone to provide a TPPM framework containing large cavities with content that is not tightly bound. In contrast, when simple, rigid, purely aromatic molecules are applied, tetraphenylmethane units assemble themselves more efficiently with well-defined interactions with the cavity content. The multiple phenyl embrace is a fundamental interaction between tetrahedral units in presented adducts **2–5**. We found that the occurrence of a given subtype of a multiple phenyl embrace is dependent on the kind of interactions introduced by the organic base. The 4PE interaction seems to be preferred for simple aromatic bases, which efficiently fill void spaces between TPPM molecules and firmly interact with them, as exemplified in adducts **2** and **3**. The 6PE interaction is formed when bases with higher affinity for dispersion interactions (adducts **4** and **5**) are used. This shows new possibilities in the tailoring of subtle interactions between tetrahedral aromatic cores.

Trends concerning the influence of the base structure find their reflection in the topology of TPPM nets. In adducts **2** and

**3**, TPPM molecules form hydrogen-bonded three-periodic nets (pcu, bcu). It seems that the high connectivity between the TPPM nodes in three-periodic nets requires a shorter distance between acid molecules, leading to the conclusion that the tendency to form three-periodic nets has in fact the same origin as the preferred formation of 4PE phenyl embraces. Topological analysis of adducts **4**, **5**, and **6** reveals that their hydrogen-bonded TPPM net (or the underlying net) is two-periodic (hxl, sql, and sql, respectively). No structure has been found to form an interpenetrated net, as was encountered in the case of adducts formed by analogous tetracarboxylic acid.<sup>39,40</sup> This is probably due to a much more diverse set of hydrogen bond patterns that the phosphonic group can form in its protonated and monodeprotonated states. The other reason is that TPPM in adducts with a proton transfer is, as a whole, two and three deprotonated, which introduces binding asymmetry.

Hydrogen bonding provided by the adjacent phosphonic groups and edge-to-face interactions originating from 6-fold phenyl embrace (6PE) were found to be cooperative in structure **4**. We proposed a new subtype of 6PE, in which these two interactions exist simultaneously in a dimer, namely a hydrogen bond-assisted phenyl embrace (HBA-PE).

## ASSOCIATED CONTENT

### Supporting Information

Crystallographic data files in CIF format, detailed synthetic procedures for TPPM and adducts with spectroscopic characterization, description of obtainment of single crystals for all structures, selected distances [Å] and angles [deg] and geometry of potential hydrogen bonds for all structures, selected NMR spectra, figures of asymmetric units, additional figures presenting specific structural features, comparison of 2D fingerprints of cocrystal **3** and acid–base adduct **4**, and decomposed 2D fingerprint plots of O···H, N···H, C···H, H···H, and C···C contacts for adducts **3** and **4**, infrared spectra discussion, description and discussion of pH-potentiometry for TPPM. This material is available free of charge via the Internet at <http://pubs.acs.org>.

## AUTHOR INFORMATION

### Corresponding Authors

\*J.K.Z. E-mail: jan.zareba@pwr.edu.pl  
\*J.Z. E-mail: jerzy.zon@pwr.edu.pl

### Notes

The authors declare no competing financial interest.

## ACKNOWLEDGMENTS

We acknowledge with thanks statutory financial support from the Faculty of Chemistry and Faculty of Mechanical and Power Engineering, Wroclaw University of Technology, Wroclaw, Poland.

## ■ REFERENCES

- (1) Jones, K. M. E.; Mahmoudkhani, A. H.; Chandler, B. D.; Shimizu, G. K. H. *CrystEngComm* **2006**, *8*, 303–305.
- (2) Taylor, J. M.; Mahmoudkhani, A. H.; Shimizu, G. K. H. *Angew. Chem., Int. Ed.* **2007**, *46*, 795–798.
- (3) Beckmann, J.; Ruttinger, R.; Schwich, T. *Cryst. Growth Des.* **2008**, *8*, 3271–3276.
- (4) Zoń, J.; Kong, D.; Gagnon, K.; Perry, H.; Holliness, L.; Clearfield, A. *Dalton Trans.* **2010**, *39*, 11008–11018.
- (5) Demadis, K. D.; Panera, A.; Anagnostou, Z.; Varouhas, D.; Kirillov, A. M.; Císařová, I. *Cryst. Growth Des.* **2013**, *13*, 4480–4489.
- (6) Dobrzańska, D.; Kubiak, J.; Janczak, J.; Zoń, J. *RSC Adv.* **2013**, *3*, 23119–23127.
- (7) Taddei, M.; Costantino, F.; Marmottini, F.; Comotti, A.; Sozzani, P.; Vivani, R. *Chem. Commun.* **2014**, DOI: 10.1039/C4CC06223J.
- (8) Bazaga-Garcia, M.; Colodrero, R. M. P.; Papadaki, M.; Garczarek, P.; Zoń, J.; Olivera-Pastor, P.; Losilla, E. R.; Leon-Reina, L.; Aranda, M. A. G.; Choquesillo-Lazarte, D.; Demadis, K. D.; Cabeza, A. *J. Am. Chem. Soc.* **2014**, *136*, 5731–5739.
- (9) Mehring, M. *Eur. J. Inorg. Chem.* **2004**, 3240–3246.
- (10) Kong, D.; Zoń, J.; McBee, J.; Clearfield, A. *Inorg. Chem.* **2006**, *45*, 977–986.
- (11) Murugavel, R.; Singh, M. P. *New J. Chem.* **2010**, *34*, 1846–1854.
- (12) Bialek, M. J.; Janczak, J.; Zoń, J. *CrystEngComm* **2013**, *15*, 390–399.
- (13) Bialek, M. J.; Zaręba, J. K.; Janczak, J.; Zoń, J. *Cryst. Growth Des.* **2013**, *13*, 4039–4050.
- (14) Desiraju, G. R. *Chem. Commun.* **1997**, 1475–1482.
- (15) Desiraju, G. R. *J. Am. Chem. Soc.* **2013**, *135*, 9952–9967.
- (16) Price, S. L. *Chem. Soc. Rev.* **2014**, *43*, 2098–2111.
- (17) Plabst, M.; Stock, N.; Bein, T. *Cryst. Growth Des.* **2009**, *9*, 5049–5060.
- (18) Mahmoudkhani, A. H.; Langer, V. *Cryst. Growth Des.* **2002**, *2*, 21–25.
- (19) Lie, S.; Maris, T.; Wuest, J. D. *Cryst. Growth Des.* **2014**, *14*, 3658–3666.
- (20) Laliberte, D.; Maris, T.; Wuest, J. D. *Can. J. Chem.* **2004**, *82*, 386–398.
- (21) Davies, R. P.; Less, R.; Lickiss, P. D.; Robertson, K.; White, A. J. P. *Cryst. Growth Des.* **2010**, *10*, 4571–4581.
- (22) Malek, N.; Maris, T.; Simard, M.; Wuest, J. D. *J. Am. Chem. Soc.* **2005**, *127*, 5910–5916.
- (23) Kim, J.; Chen, B. L.; Reineke, T. M.; Li, H. L.; Eddaoudi, M.; Moler, D. B.; O’Keeffe, M.; Yaghi, O. M. *J. Am. Chem. Soc.* **2001**, *123*, 8239–8247.
- (24) Hoffart, D. J.; Dalrymple, S. A.; Shimizu, G. K. H. *Inorg. Chem.* **2005**, *44*, 8868–8875.
- (25) Sarma, B.; Nangia, A. *CrystEngComm* **2007**, *9*, 628–631.
- (26) Boldog, I.; Domasevitch, K. V.; Baburin, I. A.; Ott, H.; Gil-Hernandez, B.; Sanchiz, J.; Janiak, C. *CrystEngComm* **2013**, *15*, 1235–1243.
- (27) Matsumoto, K.; Inokuchi, D.; Hirao, Y.; Kurata, H.; Kubo, T. *Cryst. Growth Des.* **2010**, *10*, 2854–2856.
- (28) Constable, E. C.; Eich, O.; Fenske, D.; Housecroft, C. E.; Johnston, L. A. *Chem.—Eur. J.* **2000**, *6*, 4364–4370.
- (29) Ma, L. Q.; Jin, A.; Xie, Z. G.; Lin, W. B. *Angew. Chem., Int. Ed.* **2009**, *48*, 9905–9908.
- (30) Eryazici, I.; Farha, O. K.; Compton, O. C.; Stern, C.; Hupp, J. T.; Nguyen, S. T. *Dalton Trans.* **2011**, *40*, 9189–9193.
- (31) Tan, C. R.; Yang, S. H.; Champness, N. R.; Lin, X. A.; Blake, A. J.; Lewis, W.; Schroder, M. *Chem. Commun.* **2011**, *47*, 4487–4489.
- (32) Brunet, P.; Simard, M.; Wuest, J. D. *J. Am. Chem. Soc.* **1997**, *119*, 2737–2738.
- (33) Chun, H.; Kim, D.; Dybtsev, D. N.; Kim, K. *Angew. Chem., Int. Ed.* **2004**, *43*, 971–974.
- (34) Thaimattam, R.; Sharma, C. V. K.; Clearfield, A.; Desiraju, G. R. *Cryst. Growth Des.* **2001**, *1*, 103–106.
- (35) Guo, W. Z.; Galoppini, E.; Gilardi, R.; Rydja, G. I.; Chen, Y. H. *Cryst. Growth Des.* **2001**, *1*, 231–237.
- (36) Slater, B. J.; Davies, E. S.; Argent, S. P.; Nowell, H.; Lewis, W.; Blake, A. J.; Champness, N. R. *Chem.—Eur. J.* **2011**, *17*, 14746–14751.
- (37) Fournier, J. H.; Maris, T.; Simard, M.; Wuest, J. D. *Cryst. Growth Des.* **2003**, *3*, 535–540.
- (38) Cheon, Y. E.; Suh, M. P. *Chem. Commun.* **2009**, 2296–2298.
- (39) Men, Y. B.; Sun, J. L.; Huang, Z. T.; Zheng, Q. Y. *CrystEngComm* **2009**, *11*, 2277–2278.
- (40) Men, Y. B.; Sun, J. L.; Huang, Z. T.; Zheng, Q. Y. *CrystEngComm* **2009**, *11*, 978–979.
- (41) Fournier, J. H.; Maris, T.; Wuest, J. D.; Guo, W. Z.; Galoppini, E. *J. Am. Chem. Soc.* **2003**, *125*, 1002–1006.
- (42) Thaimattam, R.; Xue, F.; Sarma, J. A. R. P.; Mak, T. C. W.; Desiraju, G. R. *J. Am. Chem. Soc.* **2001**, *123*, 4432–4445.
- (43) Basavouj, S.; Aitipamula, S.; Desiraju, G. R. *CrystEngComm* **2004**, *6*, 120–125.
- (44) Dinca, M.; Dailly, A.; Long, J. R. *Chem.—Eur. J.* **2008**, *14*, 10280–10285.
- (45) Demmer, C. S.; Krogsgaard-Larsen, N.; Bunch, L. *Chem. Rev.* **2011**, *111*, 7981–8006.
- (46) Zoń, J.; Garczarek, P.; Bialek, M. J. Synthesis of Phosphonic Acids and Their Esters as Possible Substrates for Reticular Chemistry. In *Metal Phosphonate Chemistry: From Synthesis to Applications*, Clearfield, A., Demadis, K. D., Eds.; RSC Publishing: Cambridge, U.K., 2012; pp 170–191.
- (47) Tavs, P.; Korte, F. *Tetrahedron* **1967**, *23*, 4677–4679.
- (48) Balthazor, T. M.; Grabiak, R. C. *J. Org. Chem.* **1980**, *45*, 5425–5426.
- (49) CrysAlis CCD and CrysAlis Red program, 171.31.8; Oxford Diffraction Poland, Wroclaw, Poland, 2006.
- (50) Sheldrick, G. M. *Acta Crystallogr. Sect. A: Found. Crystallogr.* **2007**, *64*, 112–122.
- (51) Brandenburg, K.; Putz, K. *Diamond, Crystal and Molecular Structure Visualization*, version 3.2i; University of Bonn, Bonn, Germany, 2012.
- (52) Blatov, V. A.; Shevchenko, A. P.; Proserpio, D. M. *Cryst. Growth Des.* **2014**, *14*, 3576–3586.
- (53) Spek, A. L. *J. Appl. Crystallogr.* **2003**, *36*, 7–13.
- (54) McKinnon, J. J.; Spackman, M. A.; Mitchell, A. S. *Acta Crystallogr., Sect. B: Struct. Sci.* **2004**, *60*, 627–668.
- (55) Spackman, M. A.; Jayatilaka, D. *CrystEngComm* **2009**, *11*, 19–32.
- (56) Spackman, M. A.; McKinnon, J. J. *CrystEngComm* **2002**, *4*, 378–392.
- (57) Wolff, S. K.; Grimwood, D. J.; McKinnon, J. J.; Turner, M. J.; Jayatilaka, D.; Spackman, M. A. *CrystalExplorer*, version 3.1; University of Western Australia: Crawley, WA, Australia, 2012.
- (58) Rathore, R.; Burns, C. L.; Guzei, I. A. *J. Org. Chem.* **2004**, *69*, 1524–1530.
- (59) It should also be noted that preparation of tetra(4-bromophenyl)methane, which involves several steps, is also non-chromatographic.
- (60) Yang, G.; Shen, C.; Zhang, L.; Zhang, W. *Tetrahedron Lett.* **2011**, *52*, 5032–5035.
- (61) Etter, M. C. *Acc. Chem. Res.* **1990**, *23*, 120–126.
- (62) The lack of phosphonic group deprotonation is confirmed by a comparison of P–O distances. Clearly, P1–O2 and P1–O3 bonds are longer (1.534(3) Å and 1.547(3) Å, respectively) than the P1–O1 bond (1.471(3) Å), indicating no delocalization of charge. In fact, these differences in bond lengths are in agreement to those previously reported (refs 12 and 13). Additionally, the lack of base protonation was reaffirmed by the C8–N1–C9 internal angle value of 118.2(3)°, which is lower than 120°, as a result of the steric effect of a lone electron pair. Gillespie, R. J. *J. Chem. Educ.* **1963**, *40*, 295–301. The conformation of the 2,2'-bipyridine molecule also provides proof for the lack of protonation. The CSD search indicates that trans conformation is the most likely scenario in cases when the 2,2'-bipyridine molecule is un- or diprotonated.
- (63) Sanna, D.; Buglyo, P.; Tomaz, A. L.; Pessoa, J. C.; Borovic, S.; Micera, G.; Garribba, E. *Dalton Trans.* **2012**, *41*, 12824–12838.

(64) Andon, R. J. L.; Cox, J. D.; Herington, E. F. G. *Trans. Faraday Soc.* **1954**, *50*, 918–927.

(65) Lazar, A. N.; Dupont, N.; Navaza, A.; Coleman, A. W. *Cryst. Growth Des.* **2006**, *6*, 669–674.

(66) The phenomenon of multiple phenyl interactions have been was reported for the first time by Muller in crystal structures of tetraphenyl arsenium and phosphonium salts: Muller, U. *Acta Crystallogr., Sect. B: Struct. Sci.* **1980**, *36*, 1071–1075. Beginning from the mid-1990s, Dance and Scudder published a series of papers in which they developed phenyl embrace systematics based upon a large number of tetrahedral units, predominantly, phosphonium salts: (a) Dance, I.; Scudder, M. *New J. Chem.* **1998**, *22* (5), 481–492. (b) Dance, I.; Scudder, M. *Chem.—Eur. J.* **1996**, *2* (5), 481–486. (c) Hasselgren, C.; Dean, P. A. W.; Scudder, M. L.; Craig, D. C.; Dance, I. G. *J. Chem. Soc., Dalton Trans.* **1997**, *12*, 2019–2027. (d) Dance, I.; Scudder, M. *J. Chem. Soc., Dalton Trans.* **1996**, 3755–3769. Since then, multiple phenyl embraces (MPEs) began to be recognized as a reliable supramolecular motif widespread in molecules containing the X-Ph<sub>n</sub> fragment, where X is any tetrahedral atom such as C, P, or Si and n = 2, 3, or 4. Depending on the number of phenyl fragments engaged in a phenyl embrace motif, many types have been identified, the most common being 4PE, a 4-fold phenyl embrace, and 6PE, a 6-fold phenyl embrace, which are the most common; phenyl embraces of a higher order (8PE or even 12PE) are also known, for instance, in various triphenylphosphine metal complexes: Dance, I.; Scudder, M. *New J. Chem.* **1998**, *22* (5), 481–492.

(67) The considered C<sub>ipso</sub> atom is the one not involved in a phenyl embrace in the case of 6PE. For 4PE, the average of two angles is calculated.

(68) Dance, I.; Scudder, M. *J. Chem. Soc., Chem. Commun.* **1995**, 1039–1040.

(69) However, to our knowledge, to date no direct comparison of 4PE and 6PE motifs with the use of this relatively new method has been conducted.

(70) CSD, version 5.35, of November 2013 using the Solid Form Module of Mercury 3.3

(71) Zolotarev, P. N.; Arshad, M. N.; Asiri, A. M.; Al-Amshany, Z. M.; Blatov, V. A. *Cryst. Growth Des.* **2014**, *14*, 1938–1949.